Available online at www.sciencedirect.com
SCIENCE DIRECT
Geochimica et Cosmochimica Acta 70 (2006) 931–946
Geochimica
www.elsevier.com/locate/gca

Stable isotope chemistry of fossil bone as a new paleoclimate indicator

Matthew J. Kohn, J. Mclver Law *

Department of Geological Sciences, University of South Carolina, Columbia, SC 29208, USA

Received 11 May 2005; accepted in revised form 31 October 2005

Abstract

During fossilization, bone is thought to recrystallize and alter chemically on timescales of kyr to a few tens of kyr, i.e., similar to the timescale for formation of soils. Therefore, C- and O-isotope compositions of bone apatite should correlate with trends in soil water composition and aridity, and serve as paleoclimate indicators. This hypothesis was tested by analyzing C- and O-isotope compositions of the CO_3 component of fossil bone apatite from mid-Oligocene through late Pleistocene units in Oregon and western Idaho, including the John Day (19.4–30.0 Ma), Mascall (15.2–15.8 Ma), and Rattlesnake (7.2–7.8 Ma) Formations, whose paleosol sequences have been studied in detail, and the Juntura (10–11 Ma), Hagerman (3.2 Ma), and Fossil Lake (<23–650 ka) fossil localities. Tooth enamel $\delta^{18}O$ values provide a baseline of meteoric water compositions. Stable isotope compositions of bone CO_3 do change in response to broad climatic trends, but show poor correlation with compositions of corresponding paleosol CO_3 at specific horizons. Instead, compositional deviations between bone and paleosol CO_3 correlate with compositional deviations with the next higher paleosol; this suggests that the timescale for fossilization exceeds one paleosol cycle. Based on stratigraphic evidence and simple alteration models, fossilization timescales are estimated at 20–50 kyr, indicating that bone CO_3 will prove most useful for sequences spanning >100 kyr. C-isotopes show negative and strong positive deviations during wet and dry climates respectively, and short-term trends correspond well with changes in aridity within the Mascall and Rattlesnake Formations, as inferred from paleosols. A proposed correction to $\delta^{18}O$ values based on $\delta^{13}C$ anomalies implies a small, ~1.5‰ increase in meteoric water $\delta^{18}O$ during the late Oligocene global warming event, consistent with a minimum temperature increase of ~4 °C. A strong inferred decrease in $\delta^{18}O$ of 4–5‰ after 7 Ma closely parallels compositional changes in tooth enamel, and reflects a doubling in the height of the Cascade Range.

1. Introduction

Unlike marine environments, which can have essentially continuous deposition of sediments and biogenic materials over thousands to millions of years, deposition and preservation in continental environments is commonly sporadic. To maximize recovery of useful paleoclimate information, stable isotope geochemists employ numerous terrestrial climate and ecological proxies, including ice cores, groundwater, speleothems, tree rings, lacustrine sediments, and organic compounds, teeth, shells, and pedogenic carbonates, clays, and oxides (e.g., Swart et al., 1993; Shanley et al., 1998; Koch, 1998). However, the variety of available proxies generally decreases with increasing time, so for times older than ~1 Ma, geochemical proxies for terrestrial climate are principally limited to fossil teeth, shells, and pedogenic minerals. These are not always uniformly distributed in either space or time, so there is a continuing need to develop other geochemical proxies for terrestrial paleoclimate.

Stable isotopes of fossil bone represent a nearly unexplored resource of paleoclimate information. Fossil bone fragments have certain advantages over other materials—they are more common and expendable than fossil teeth, yet are readily recognized and collected in the field. Furthermore, fossil bone fragments may allow investigation of any relationships between climate change and biotic evolution in fossiliferous sequences where pedogenic materials are lacking. Here, the stable isotope geochemistry of the CO_3 component of fossil bone mineral is compared to paleosol and fossil tooth isotope records, and shown to

* Corresponding author. Fax: +1 803 777 6610.
E-mail address: mjk@geol.sc.edu (J.M. Law).

0016-7037/$ - see front matter © 2005 Elsevier Inc. All rights reserved.
doi:10.1016/j.gca.2005.10.023

be a useful proxy for aridity and soil water composition, complementing other proxies in older strata.

2. Chemical and physical systematics of bone

The physical and chemical characteristics of modern vs. fossil bone are discussed first because of their influence on the expected isotopic patterns in fossils. Bone mineral is calcium-phosphate, with a crystal structure similar to apatite [$Ca_5(PO_4)_3(OH, F, Cl)$]. However, the mineral in biogenic phosphatic tissues, such as bone, dentin, and enamel, contains significant substitution of CO_3 into the PO_4 and OH sites. Bone mineral is additionally unusual chemically because it contains more CO_3 than other phosphatic tissues, and virtually no OH, F, or Cl (Driessens and Verbeeck, 1990; Pasteris et al., 2004). These characteristics may be physiologically advantageous for two reasons. First, bone mineral must be remodeled, and in comparison to a non-remodeled tissue such as enamel, CO_3-rich, OH-deficient bone "apatite" has orders of magnitude greater solubility (Driessens and Verbeeck, 1990; Pasteris et al., 2004). Second, sharing of OH groups between bone mineral and collagen produces stronger mineral-collagen bonds (Pasteris et al., 2004; Wilson et al., 2005). Although bone mineral contains significant Na and Mg (roughly 0.5 wt%), it is notably lacking in REEs (Driessens and Verbeeck, 1990).

Physically, bone mineral forms nano-crystalline plates or ribbons, with length-width dimensions of a few tens of nm. Estimates of thickness vary from at most ~4 nm (as determined via transmission electron microscopy; e.g., Rubin et al., 2004) to less than 1 nm (as determined via atomic force microscopy; Eppell et al., 2001). Differences in estimated thickness may simply reflect differences in sample preparation (e.g., coarsening during extraction for some TEM studies) and/or limits to the spatial resolution of TEM imaging (Eppell et al., 2001; Rubin et al., 2003). These thicknesses correspond crystallographically to at most a few unit cells, to $\leqslant$1 unit cell for thicknesses as estimated via AFM.

Upon burial, fossilization, and degradation of collagen, bone mineral becomes physically and chemically unstable, and its characteristics change radically. Structurally and chemically, it transforms to dahllite or francolite (carbonate hydroxy- or fluor-apatite), with several orders of magnitude increases in REE and U contents (e.g., see Kohn et al., 1999; Trueman and Tuross, 2002), a factor of 2 decrease in CO_3 content (Wright and Schwarcz, 1996), orders of magnitude decrease in solubility (Driessens and Verbeeck, 1990), and growth and infilling of authigenic minerals, including phosphates (Trueman et al., 2004). Insofar as bone mineral is unstable outside its collagen matrix (Pasteris et al., 2004; Wilson et al., 2005), chemical and mineralogical alteration initiates within a few years of burial and proceeds until collagen is completely degraded (Tuross et al., 1989; Trueman and Tuross, 2002; Trueman et al., 2004). Complete recrystallization and chemical alteration are believed to occur within a few kyr to tens of kyr, as indicated both by the presence of fossilized diffusion gradients in trace elements (Millard and Hedges, 1999; Trueman and Tuross, 2002), and the common occurrence of completely fossilized (collagen-absent) bones from the last glacial maximum, for example, the <25 ka fossils from Fossil Lake, Oregon (Martin et al., 2005). However, once fossilized and recrystallized, bones retain their (altered) compositions for millions of years, as indicated by trace element-based provenance studies (Trueman and Benton, 1997; Staron et al., 2001; Metzger et al., 2004), Sr systematics in marine fossils (Wright et al., 1984; Staudigel et al., 1985), and comparability of fossil bone crystallinity to enamel (Ayliffe et al., 1994), which preserves isotopic signatures for tens of Myr (Wang and Cerling, 1994; Koch, 1998; Kohn and Cerling, 2002).

With respect to stable isotope systematics, dissolution/reprecipitation or recrystallization of bone crystallites is expected to reset the isotope composition of all components to whatever the prevailing composition is within the soil. For PO_4, the fossil itself dominates the source, and if alteration occurs abiotically, then the isotope composition of PO_4 will not change. However if bacteria are involved, for example in degrading collagen, then biotic PO_4 recycling can readily change $\delta^{18}O$ values (e.g., Blake et al., 1997, 1998; Zazzo et al., 2004a). Because PO_4 recycling via bacteria is difficult to quantify, the isotopic alteration potential of bone PO_4 is debated (see summary of Kohn and Cerling, 2002; Trueman et al., 2003; Zazzo et al., 2004b). In contrast to PO_4, CO_2 concentrations in soils are controlled not via fossil dissolution, but by degradation of soil organic matter. Thus, the possibility of retaining original isotopic compositions of the CO_3 component in bones is remote. This expectation is confirmed by isotopic studies that clearly demonstrate $\delta^{13}C$ resetting of bone mineral for typical samples of Pleistocene and younger age (Land et al., 1980; Schoeninger and Deniro, 1982; Nelson et al., 1986; Lee-Thorpe and van der Merwe, 1991; Wright and Schwarcz, 1996). This view of fossilization is meant as a general guideline rather than a rigid and universal rule, and is certainly refuted in rare instances by well-preserved, >1 Ma collagen and other soft tissues; however such fossils are not common, and were not the target of this study.

Of importance to this study, the timescale for formation of many paleosols and pedogenic minerals is a few kyr to a few tens of kyr, at least for Tertiary paleosols of Oregon (Retallack et al., 1999, 2002, 2004; Retallack, 2001, 2004), i.e., subequal to the timescale for fossilization. Furthermore, the stable isotope composition of fossil bone CO_3 in some settings has been shown to parallel local soil and diagenetic carbonates (Barrick and Showers, 1994). Thus, bone mineral should in principle recrystallize and adopt an isotope composition for its CO_3 component reflective of pedogenic conditions. If so, then because paleosol carbonate composition proves useful as a paleoclimate proxy (Cerling and Quade, 1993), so too should the CO_3 component of fossil bone.

3. Samples

Retallack et al. (2004) collected a suite of Oligocene to early Miocene paleosols from central Oregon, spanning 28.7–19.2 Ma (Fig. 1). Biostratigraphy throughout the sequence, and precise (typically better than ±100 kyr) $^{40}Ar/^{39}Ar$ ages plus magnetic reversal data for the 28.7–24.3 Ma interval yield a linear sedimentation rate and an estimate for the age of each paleosol (Retallack, 2004; Retallack et al., 2004). These data indicate a ~40 kyr cyclicity per 3 paleosols (Retallack et al., 2004), or 10–15 kyr/paleosol. Many of these paleosols contain fossil bone fragments, which were analyzed in this study to provide one of the main data sets. Retallack et al. (2004) also collected paleosol carbonate nodules from stratigraphically equivalent sequences, spanning 28.7–22.6 Ma, and analyzed them for carbon and oxygen isotope compositions. Combination of datasets permits comparison of the stable isotopes of fossil bone CO_3 vs. paleosol carbonate. However, most of the paleosol carbonates were collected ~4 km from the bulk of the fossil bone samples. Thus, any stratigraphic measurement errors or differences in sedimentation rates at different sites could lead to stratigraphic miscorrelation.

Two points are noteworthy regarding the paleosol sequences and the bone samples. First, the time encompassed by the bone-bearing paleosols can be estimated from the stratigraphic level of each paleosol that contains an analyzed bone fragment and the level of the next higher paleosol (data to the nearest 0.1 m from Retallack, 2004 and Retallack et al., 2004). On average this time is within the 10–15 kyr/paleosol time range for other paleosols, i.e., there is no systematic bias for fossil bone-bearing paleosols vs. other paleosols. Second, the ~40 kyr cyclicity of paleosol formation is matched by major, brief (<15 kyr) negative excursions in paleosol $\delta^{18}O$ and $\delta^{13}C$ values, related to cyclic changes in climate (Retallack et al., 2004). Consequently, even small stratigraphic errors could lead to erroneous compositional comparisons between bone fragments and paleosol carbonates, particularly for the compositionally anomalous paleosols.

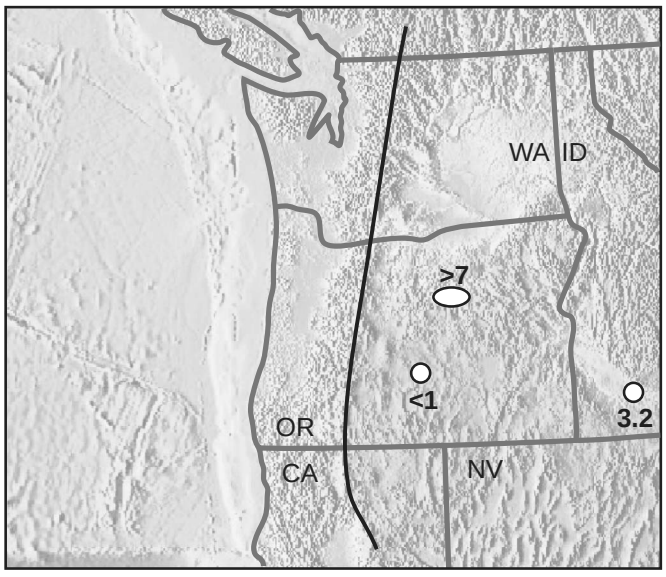

Fig. 1. Topographic map of Pacific Northwest, US, showing locations of samples (numbers are ages in Ma); solid line is the trend of the Cascade volcanic arc.

To complement the bone samples from paleosols, fossil bone fragments were also collected from Oligocene to Pliocene strata in Oregon and Idaho that lack paleosol carbonate data, but contain fossil tooth enamel whose PO_4 component was analyzed for oxygen isotope compositions (Kohn et al., 2002; Kohn and Fremd, in press; Fig. 1). Because compositions of tooth enamel and surface water correlate, this approach permits broad comparison of the stable isotope record of fossil bone vs. (paleo-) water. Stratigraphically and chronologically, the Oligocene samples (28.8–30.0 Ma) extend the transects of Retallack (2004) and Retallack et al. (2004) to lower stratigraphic levels; ages assume the same linear sedimentation rate deduced for the 28.7–24.3 Ma interval. Ages for the Miocene and Pliocene samples are based on biostratigraphy plus precise (typically better than ±100 kyr) $^{40}Ar/^{39}Ar$ ages on intercalated tuffs (see Kohn et al., 2002; Appendix A). Pleistocene samples from Fossil Lake Oregon occur in terrestrial gravels, and are dated by tephrochronology on intercalated ash beds at <23 to ~650 ka (Martin et al., 2005). Samples available for analysis were all fragments, taxonomically unidentifiable more specifically than class (mammals and fish) except for fossil teeth of *Equus* sp. from Fossil Lake.

Fossil bone was sampled simply by sawing out pieces with a slow-speed microsaw. Each piece was classified according to texture. The terms "compact" vs. "spongy" are used here to distinguish cortical vs. cancellous bone that had relatively low vs. high intrinsic porosity prior to fossilization. These two types of bone were classified and analyzed separately to see whether original porosity influenced susceptibility to alteration and hence isotope compositions and timescales of fossilization. Each sample was analyzed following the procedures of Koch et al. (1997). Further analytical details and raw data are detailed in Appendix A; statistical results are summarized in Tables 1 and 2. For F tests and linear regressions (Table 2), statistical significance is based on $p \leqslant 0.05$, $\alpha \geqslant 0.95$, and/or slopes that are different from 0.0 at ±2 s. Alternative regression approaches (e.g., reduced major axis regressions) do not change the main conclusions of this study.

4. Results

4.1. Bone–paleosol comparisons

In general, there is little difference in mean compositions or in data scatter for coexisting compact vs. spongy bone

Table 1
Population statistics for fossils from Central Oregon and Southwestern Idaho, USA

Material	Age (Ma)	$\delta^{13}C$ Mean ± 1 s	$\delta^{18}O$ Mean ± 1 s	n	Corrected $\delta^{18}O$ ± 1 SE
Compact	28.8–30.0	−10.97 ± 0.73	17.79 ± 1.09	30	18.5 ± 0.3
Spongy	28.8–30.0	−10.79 ± 0.60	17.19 ± 0.99	10	17.7 ± 0.4
Compact	19.4–28.7	−10.39 ± 0.76	19.33 ± 1.21	95	19.6 ± 0.2
	26.0–28.7	−10.54 ± 0.77	18.85 ± 1.04	57	19.1 ± 0.2
	19.4–25.0	−9.67 ± 0.66	20.81 ± 1.01	15	20.4 ± 0.4
Spongy	19.4–28.7	−10.14 ± 0.85	19.71 ± 1.24	65	19.7 ± 0.2
	26.0–28.7	−10.18 ± 0.81	19.32 ± 1.16	38	19.1 ± 0.3
	19.4–25.0	−9.77 ± 0.84	20.81 ± 0.82	15	20.5 ± 0.4
Compact	15.2–15.8	−11.15 ± 1.22	20.60 ± 1.03	14	22.7 ± 0.5
Compact (mammal)	10–11	−8.67 ± 1.12	20.33 ± 0.86	11	17.4–19.8
Compact (fish)	10–11	04.09 ± 5.22	20.16 ± 0.57	12	Not calculated
Compact	7.2–7.8	−10.60 ± 0.73	19.89 ± 1.44	13	20.5 ± 0.5
Spongy	7.2–7.8	−10.36 ± 0.71	19.65 ± 1.31	20	20.0 ± 0.4
Compact	3.2	−8.26 ± 0.77	19.90 ± 1.48	6	16.2 ± 0.8
Spongy	3.2	−7.20 ± 0.89	20.16 ± 1.24	7	15.1 ± 0.7
Compact	0.025–0.6	−2.0 ± 0.70	27.01 ± 0.73	21	16.1 ± 0.9
Dentine	0.025–0.6	−5.81 ± 2.00	20.96 ± 0.77	21	14.0 ± 0.8

Note. The marine record shows an important climate transition between 25 and 26 Ma (e.g., Zachos et al., 2001), so compositional comparison to John Day paleosols were split out for times before and after this transitional period. Marine C-isotope compositions used for corrections were: 0.75‰ (>26 Ma), 1.0‰ (19–25 Ma), 1.5‰ (15–16 Ma), 1.0‰ (7–11 Ma), and 0.0‰ (3.2–0.025 Ma). For paleosols, C-isotope compositions (V-PDB) are −9.1 ± 1.0‰ (28.7–22.6 Ma), −9.3 ± 1.0‰ (28.7–26.0 Ma), and −8.8 ± 0.9‰ (25.0–22.6 Ma), and O-isotope compositions (V-SMOW) are 17.4 ± 1.6‰ (28.7–22.6 Ma), 16.5 ± 1.3‰ (28.7–26.0 Ma), and 18.7 ± 1.3‰ (25.0–22.6 Ma). The correction to the Juntura Formation mammal fossils could be overestimated if their $\delta^{13}C$ values are influenced by exchange with interlayered high $\delta^{13}C$ lacustrine deposits; consequently a range of possible corrected compositions is listed. The error estimate for the corrected compositions assumes standard errors for raw compositions.

Table 2
F tests and linear regression statistics of compact bone, spongy bone, and paleosol carbonate compositions

Comparison/regression	*F* test p, $\delta^{13}C$	*F* test p, $\delta^{18}O$	$\delta^{13}C$ r^2, F, α	Slope ± 1 s	$\delta^{18}O$ r^2, F, α	Slope ± 1 s
Compact vs. spongy bone, JODA paleosols	0.13	0.15				
Compact vs. paleosol JODA paleosols	<0.01	<0.01	0.000, 0.03, 0.1	0.02 ± 0.09	0.000, 0.04, 0.2	−0.02 ± 0.10
Spongy vs. paleosol JODA paleosols	0.09	0.025	0.000, 0.00, 0.02	0.00 ± 0.14	0.016, 0.4, 0.5	0.11 ± 0.18
(Bone–paleosol) vs. (next paleosol–paleosol) JODA paleosols			0.30, 46.0, >0.99	0.44 ± 0.07	0.27, 38.9, >0.99	0.55 ± 0.09
Bone vs. time, Mascall Fm			0.54, 25.9, >0.99	5.3 ± 1.0	0.07, 1.8, 0.8	−1.6 ± 1.2
Bone vs. time, Rattlesnake Fm			0.40, 12.0, 0.98	−2.5 ± 0.9	0.03, 3.0, 0.4	−1.4 ± 2.3

F tests between compositions of paleosols vs. bone are 2-sided and cover the entire time range represented by the paleosols, i.e., 22.6–28.7 Ma. Exact comparison for only the correlated strata (i.e., a small subset of the paleosols) yields similar results for compact bone–paleosol ($p < 0.02$) and compact bone-spongy bone ($p = 0.1$–0.3), but suggests more similarity for spongy bone–paleosol (0.12–0.32).

(Tables 1 and 2). Compared to paleosol carbonate, mean $\delta^{13}C$ and $\delta^{18}O$ values for bone CO_3 are shifted by −1.5‰ for C-isotopes and +2.2‰ for O-isotopes (Tables 1 and 2; Figs. 2 and 3). Compositional differences in the means are not surprising because the comparison is between CO_3 in different minerals—calcite in paleosols vs. francolite/dahllite in fossil bone. However, there is poor correlation between the stable isotope compositions of fossil bone vs. coexisting paleosol carbonate (Figs. 2A and B; Table 2): regression slopes are not significantly different from zero, and $\alpha \leqslant 0.5$ (Table 2). These results suggest that there is not a 1:1 correspondence in the timescale for paleosol carbonate formation and bone fossilization. Insofar as *F* tests reveal that the degree of scatter in fossil bone compositions is significantly smaller than for paleosol carbonate, particularly for compact bone (Tables 1 and 2; Figs. 2A and B), the timescale for bone fossilization and isotopic alteration is likely longer than for formation of paleosol carbonate, i.e., greater than 10–15 kyr.

This hypothesis was tested by plotting the deviation between the composition of each bone fragment and its corresponding (nth) paleosol [i.e., Δ(bone − paleosol)] vs. the deviation between the compositions of the nth and next higher ($n + 1$st) paleosol [i.e., Δ(next paleosol − paleosol)] (Figs. 2C and D). A significant correlation would indicate that bone compositions in the nth paleosol are influenced by the composition of the $n + 1$st paleosol, and that fossilization extended at least partially into the next paleosol cycle. Most data correlate strongly (Fig. 2; >99% confidence; Table 2) with a slope of ~0.5. This slope suggests that roughly 50% of the alteration had occurred prior to formation of the next higher paleosol. Including the $n + 2$nd paleosol does not significantly improve regression statistics, suggesting a rapidly diminishing influence of higher paleosols.

Data from one horizon clearly do not fall on the main composition trend (gray symbols in Fig. 2). This deviation is likely due to a compositionally anomalous overlying

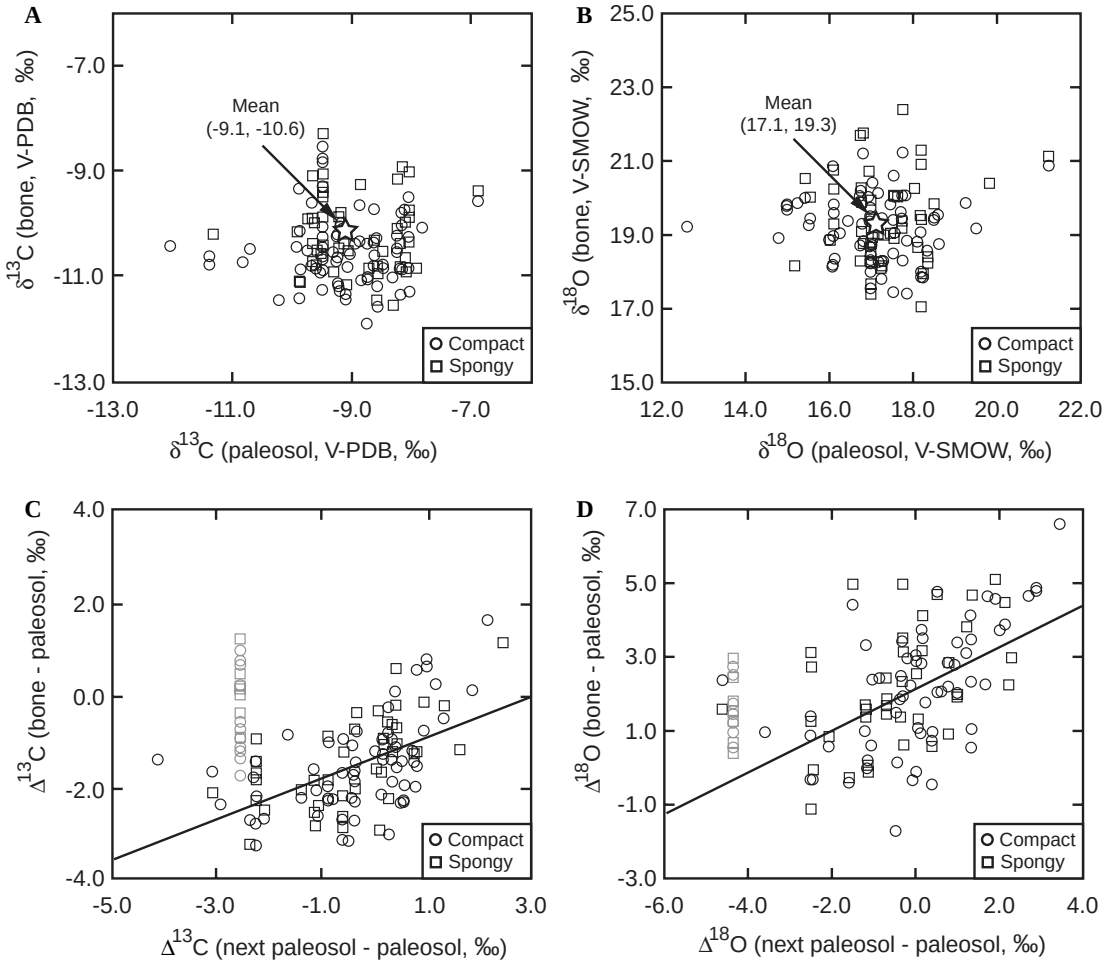

Fig. 2. (A, B) Plot of bone composition vs. paleosol composition, showing smaller scatter for bone vs. paleosol, and poor correlation. There is no significant difference between spongy vs. compact bone compositions. (C, D) Plot of difference between bone CO_3 and paleosol carbonate compositions vs. difference between paleosol and next higher paleosol carbonate compositions. Significant correlations for carbon and oxygen indicate that stable isotope compositions of bone CO_3 reflect soil conditions, but encode a greater amount of time than a single paleosol. Gray symbols indicate that the next higher paleosol has an extreme composition, so plotting position is sensitive to minor stratigraphic miscorrelation and possible short timescale for paleosol formation. Lines show trends of linear regressions.

paleosol [i.e., unusual value for Δ(next paleosol − paleosol)]. If either there is an error in stratigraphic correlation, or that paleosol formed too quickly (e.g., less than a few kyr), then soil water compositions during its formation would not have affected these bone fragments during fossilization, and the comparison is spurious. Based on distinctive values for depth to calcic horizons, and a small distance from the main marker horizon, stratigraphic miscorrelation seems unlikely. However, stratigraphic thicknesses do imply only a 5 kyr difference in age between this paleosol and the next overlying paleosols, so rapid vs. slow rates of paleosol formation vs. fossilization may well explain these specific data.

4.2. Carbon isotope composition trends

The approximate constancy of bone $\delta^{13}C$ between 30 and 7 Ma (Fig. 3) is similar to the compositional behavior of paleosols and the marine record. A possible small increase in paleosol $\delta^{13}C$ between 29 and 24 Ma is consistent with an increase in bone $\delta^{13}C$ values. There are also small, but well-resolved trends towards lower $\delta^{13}C$ values at 15–16 Ma and towards higher $\delta^{13}C$ values at 7–8 Ma (Fig. 4). At 10–11 Ma, radical differences in $\delta^{13}C$ for mammals (range = −4.2 to −10.7) vs. fish (range = −5.1 to +9.4) reflect different environments and sedimentary materials—the mammal fossils all derive from terrestrial deposits, whereas the fish are from lacustrine diatomaceous deposits. Intracontinental freshwater lakes and diatoms commonly have high $\delta^{13}C$ values, so the fish compositions are not unusual. However, most mammal fossils show limited evidence of enriched ^{13}C derived from lacustrine beds (likely < 2‰), despite intimate interfingering of disparate strata on a meter to sub-meter scale, age differences ⩽30–50 kyr, and $\Delta^{13}C_{terrestrial–lacustrine}$ approaching 20‰. After 7 Ma, a major trend towards higher $\delta^{13}C$ is clearly decoupled

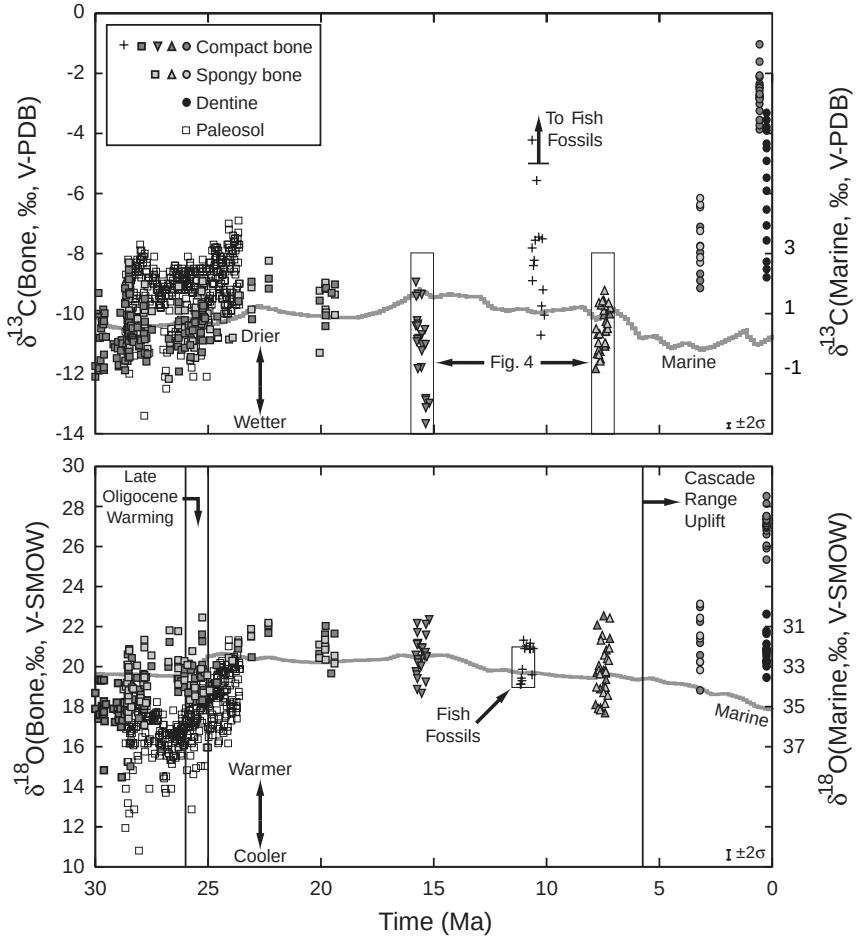

Fig. 3. Plot of $\delta^{13}C$ and $\delta^{18}O$ composition vs. time for Oligocene paleosol carbonate (Retallack et al., 2004) and fossil bone and dentin CO_3. Prior to 7 Ma $\delta^{13}C$ values of bones and teeth broadly correspond with marine isotopes, except for a negative trend between 15 and 16 Ma, reflecting increased moisture and/or a canopy effect, and a positive trend at 7–8 Ma, indicating increased aridity (see Fig. 4). $\delta^{18}O$ and $\delta^{13}C$ values of bone and dentin CO_3 progressively rise after 7 Ma due to increased aridity attending uplift of the Cascade Range. Note that $\delta^{18}O$ values for 3.2 Ma samples are increased by 1.0‰ to account for longitudinal differences in modern water compositions in central Oregon vs. Idaho. For Fossil Lake (<1 Ma), carbon isotope data for bone have been offset from dentine for clarity.

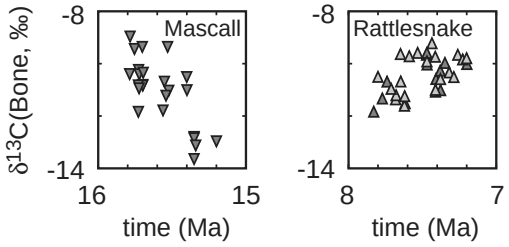

Fig. 4. Detailed plot of $\delta^{13}C$ vs. time for Mascall and Rattlesnake Formations, illustrating significant sub-Myr trends.

from the marine record. The data from Fossil Lake reach −1‰, which implies paleosol carbonate $\delta^{13}C$ values > 0‰.

4.3. Oxygen isotope composition trends

Oxygen isotope trends in fossil bone since 30 Ma are less directly correlated with paleosols or the marine record. A small increase in bone $\delta^{18}O$ is resolved across the late Oligocene warming trend indicated by marine records, and is consistent with an expected increase in temperature, and with a trend towards higher $\delta^{18}O$ values in the paleosols. However, most other bone compositions show either approximately constant or increasing $\delta^{18}O$ (with increasing $\delta^{13}C$). This behavior contrasts markedly with tooth enamel records from fossil equid and rhino teeth that show a clear trend towards decreasing $\delta^{18}O$ since 7 Ma (Kohn et al., 2002; Kohn and Fremd, in press). Interestingly, for the 10–11 Ma samples, despite radically different $\delta^{13}C$ values (a 2-sided t test yields $p = 3 \times 10^{-6}$), fish and mammal bones have indistinguishable $\delta^{18}O$ values ($p = 0.681$), suggesting common source water compositions.

5. Interpretations

5.1. Timescales of fossilization

For the John Day samples, if 50% fossilization occurs during a paleosol cycle, then the slope of the deviations

in isotope compositions should be 0.5, as observed. This linear model of bone alteration and recrystallization then yields a timescale of fossilization of 20–30 kyr. An alternative model in which fossilization rates decrease exponentially implies a characteristic time-constant of $\sim 6 \times 10^{-5}\ \mathrm{yr}^{-1}$, or ~50 kyr to effect 95% alteration and recrystallization. Because there is no significant difference in the population statistics for compact vs. spongy bone, the timescales of fossilization for both are indistinguishable. In general, longer fossilization times of hundreds of kyr are ruled out by the common occurrence of fully fossilized materials from the last glacial maximum (<25 ka), the absence of extensive isotopic interaction in the Juntura Formation between mammal bones and high $\delta^{13}C$ diatomaceous deposits with maximal age disparities of 30–50 kyr, and resolvable trends in fossil bone compositions on timescales much less than 1 Myr (Fig. 4). Although specific instances of unfossilized and/or subfossil material older than 50 ka are known elsewhere, the data from Oregon generally support a more typical timescale of fossilization of 20–50 kyr.

5.2. Carbon isotope compositions

Carbon isotope compositions are commonly used to monitor past biomass proportions of C3 and C4 (±CAM) plants because of the large ^{13}C-enrichment in C4 and CAM plants and corresponding soils (e.g., O'Leary, 1988; Farquhar et al., 1989; Cerling and Quade, 1993; Koch, 1998). However, C4 and CAM plants likely never influenced compositions significantly in central Oregon, southeastern Oregon, and southwestern Idaho. CAM plants have been present in the world since the early Mesozoic (Keeley and Rundel, 2003) and C4 plant macrofossils occur in North American strata by 12 Ma (see Kohn and Cerling, 2002, for discussion). Both CAM and C4 plants are better adapted than C3 plants to low p_{CO_2}, and are moderately to strongly drought-tolerant. Thus (seasonal) aridity and low CO_2 levels would be expected to favor CAM and C4 plants relative to C3 plants. Today, southeastern Oregon and southwestern Idaho have about as low a CO_2 level and as dry a climate as ever occurred in the Cenozoic, yet a negligible C4 + CAM plant biomass occurs there today. For example, Fields (1996) tabulates more than 200 C3 species in that region but only 1 CAM species and 3 C4 species; all grasses he observed (~20 species) are C3. Thus, changes in C3–C4–CAM biomass ratios do not appear responsible for observed changes to bone $\delta^{13}C$ values.

Instead, for ecosystems dominated by C3 plants, the $\delta^{13}C$ of paleosols correlates with precipitation and plant productivity, and with the difference between potential evapotranspiration and mean annual precipitation (Amundson et al., 1988, 1989; Quade et al., 1989; Cerling and Quade, 1993). Lower vs. higher $\delta^{13}C$ indicates wetter vs. drier conditions. For example the 600 kyr trend towards lower $\delta^{13}C$ at 15–16 Ma may reflect increasing moisture during the mid-Miocene climatic optimum, whereas the 600 kyr trend towards higher $\delta^{13}C$ at 7–8 Ma may correspond with drying. Both interpretations are consistent with paleosol sequences that indicate unusually wet conditions during deposition of the mid-Miocene Mascall Formation (Retallack et al., 1999; Bestland et al., 2005), and a drying trend during deposition of the late Miocene Rattlesnake Formation (Retallack et al., 2002). The increasingly high $\delta^{13}C$ values in the Plio-Pleistocene correspond with increasing aridity driven by renewed volcanism and uplift of the Cascade Range, commencing after 7 Ma (Kohn et al., 2002). The highest $\delta^{13}C$ values in the late Pleistocene are comparable to modern paleosol carbonate from C3-dominated deserts (Amundson et al., 1988, 1989; Quade et al., 1989; Cerling and Quade, 1993); a high-desert scrubland ecology is present today in Oregon and Idaho.

5.3. Oxygen isotope compositions

Comparison of oxygen isotope compositions of fossil bone CO_3 vs. coeval tooth enamel PO_4 (Fig. 5) shows that the two materials are not in oxygen isotope equilibrium. In biogenic phosphates, CO_3 should be ~8‰ enriched compared to PO_4 (Bryant et al., 1996; Iacumin et al., 1996); instead prior to 6 Ma, fossil bone CO_3 is only ~6‰ enriched compared to enamel PO_4. This level of enrichment is consistent with diagenetic overprinting of CO_3. Typically, mammal body water is ~6‰ enriched over local surface water (e.g., Kohn, 1996; Kohn and Cerling, 2002). So if diagenesis proceeded at the same temperature as a mammal (37 °C), but with water that is 6‰ lower, the $\delta^{18}O$ of bone CO_3 would be only 2‰ higher than PO_4. However, diagenesis must occur at a much lower temperature (e.g., estimated mean annual temperatures for the mid- to late-Cenozoic of Oregon are 10–20 °C; see summary of Kohn et al., 2002). Assuming a 15 °C diagenetic temperature and a temperature-dependence of oxygen isotope fractionations for bone CO_3 that parallels carbonates (Kim and O'Neil, 1997), the $\delta^{18}O$ of bone CO_3 would be an additional 4‰ higher. That is, bone CO_3, if purely diagenetic, should have values ~6‰ higher than enamel PO_4, as generally observed for much of the isotope record.

In terms of oxygen isotope trends, lower vs. higher $\delta^{18}O$ in terrestrial records commonly indicates lower vs. higher soil water $\delta^{18}O$, which correlates with lower temperatures and/or increased moisture vs. higher temperatures and/or increased aridity. For example, the ~2‰ increase in $\delta^{18}O$ in the late Oligocene likely reflects an increase in temperature associated with global warming (e.g., Zachos et al., 2001). Because continental climate variations are commonly magnified compared to the oceans, a moderate isotopic shift in Oregon in the late Oligocene is expected. In contrast, in view of the evidence from tooth enamel records for decreased $\delta^{18}O$ values for meteoric water since 7 Ma

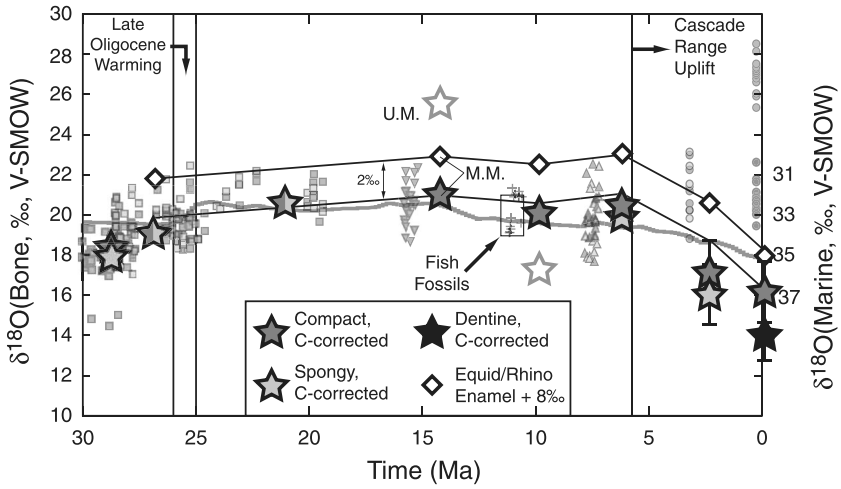

Fig. 5. Plot of $\delta^{18}O$ values for C-corrected bone CO_3 vs. time showing a strong depletion in meteoric water $\delta^{18}O$, consistent with oxygen isotope data from fossil tooth enamel PO_4 (data from Kohn et al., 2002; Kohn and Fremd, in press). M.M., middle Mascall Formation (equivalent to the lower part of the transect sampled for bone stable isotopes, and the source of tooth enamel analyzed by Kohn et al., 2002); U.M., upper Mascall Formation. Data from Fig. 3 shown for reference. Symbols for C-corrected values and tooth enamel are displaced in time so that raw data are not masked. Error bars for C-corrected $\delta^{18}O$ values are based on propagation of standard errors; error bars are subequal to the size of the symbols for samples older than 3.2 Ma, and are shown for youngest corrected values. Gray stars indicate corrected values that may be affected adversely by a canopy effect (upper Mascall at ~15.5 Ma) and isotopic exchange with high $\delta^{13}C$ interbedded lacustrine deposits (Juntura at 10–11 Ma).

(Kohn et al., 2002), and the overall cooling trend recorded in the oceans (e.g., Zachos et al., 2001; Fig. 2), the relatively high $\delta^{18}O$ values for Plio-Pleistocene bone must in part reflect evaporative enrichment in soil water ^{18}O attending increased aridity.

Paleo-soil water compositions may possibly be retrieved through a semi-quantitative correction of bone $\delta^{18}O$ values, proposed here to account for evaporative enrichment. This correction is based on the positive correlation between $\delta^{18}O$ and $\delta^{13}C$ that has been observed in modern paleosols in C3-dominated ecosystems of the western US (Amundson et al., 1989; Quade et al., 1989), and that is evident in Eocene and Oligocene paleosols from Wyoming and central Oregon, respectively (Clyde et al., 2001; Retallack et al., 2004). Clearly such a model will not work for mixed C3–C4 ecosystems, where changes in ^{13}C reflect proportions of C3/C4 plant biomass and are not necessarily coupled to productivity and soil moisture. Similarly, if $\delta^{13}C$ values are influenced by diagenetic interaction with high $\delta^{13}C$ lacustrine deposits, as appears evident for at least 2 samples from the Juntura Formation, then corrections to $\delta^{18}O$ values may be overestimated. For this reason, a range of corrections is proposed for the Juntura samples, and the least corrected (lowest $\delta^{13}C$) samples likely best represent this time. At the other isotopic extreme, closed canopy forests with unusually low $\delta^{13}C$ may also be inappropriate for this correction as their isotopic compositions reflect physical and biological factors other than soil moisture. Values for bone $\delta^{13}C$ in the upper part of the Mascall Formation are sufficiently low ($<-13‰$) that a canopy effect may be inferred. Therefore, the highest $\delta^{13}C$ samples, from the same strata as fossil teeth analyzed by Kohn et al. (2002), likely best represent this interval.

For C3-only ecosystems, paleosol datasets yield slopes of 1.2–1.6‰ ($\delta^{18}O$)/1‰ ($\delta^{13}C$) (Amundson et al., 1989; Quade et al., 1989; Clyde et al., 2001; Retallack et al., 2004). As long as ecosystems are known to be virtually C4- and CAM-absent, as they are in Oregon and in the middle to lower Tertiary, these correlations may be largely ascribable to changes in productivity and vegetation density in response to changes in overall rainfall and soil moisture content. For example, decreased precipitation tends to cause moisture stress in plants (higher $\delta^{13}C$ for plants and soil organic matter), increased evaporative enrichment (higher soil $\delta^{18}O$), and decreased overall productivity (higher soil $\delta^{18}O$ and $\delta^{13}C$). For this correction, the dataset of Retallack is geographically and temporally most relevant, and yields a regressed slope of $1.25 \pm 0.06‰(\delta^{18}O)/‰$ ($\delta^{13}C$) ($\pm 1s$; $r^2 = 0.56$). That slope is used to correct bone $\delta^{18}O$ values to a common $\delta^{13}C$ baseline, specifically to a constant $\delta^{13}C$ offset relative to the marine C-isotope composition (which changes slightly because of secular changes to atmospheric $\delta^{13}C$). A larger or smaller slope would yield a lower or higher corrected $\delta^{18}O$ value. The correction proposed here is:

$$\delta^{18}O_{C\text{-corrected}}(‰) = \delta^{18}O_{bone} - 1.25 \cdot (\delta^{13}C_{bone} + 11.0 - \delta^{13}C_{marine}) \quad (1)$$

This approach yields $\delta^{18}O$ values that are "C-corrected" to a common aridity that can then be compared to each other and to tooth enamel trends. The C-corrected composition is interpreted as a meteoric water composition (i.e., soil water prior to evaporative enrichment). For compositions in Table 2, the correction essentially registers data to the average aridity during deposition of the John Day

Formation between 19 and 24 Ma (because $\delta^{13}C_{marine} \sim 1‰$ and $\delta^{13}C_{bone} \sim -10‰$, yielding a correction of 0). Eq. (1) allows comparison of different times with different aridities and atmospheric $\delta^{13}C$ values. For example, at 3 Ma, $\delta^{13}C_{marine}$ is ~0.0‰. Thus, in comparison to 19–24 Ma samples, a hypothetical 3 Ma fossil with $\delta^{13}C_{bone} = -10‰$ would be corrected by $-1.25 \cdot (+1.0)‰ = -1.25‰$. The downward correction occurs because a −10‰ fossil at 3 Ma is less depleted in ^{13}C relative to atmospheric CO_2 than a −10‰ fossil at 19–24 Ma (i.e., $\Delta^{13}C_{bone\text{-}marine}$ would be −10‰ at 3 Ma vs. −11‰ at 19–24 Ma). The smaller depletion indicates drier conditions at 3 Ma, and isotopic correction for greater evaporative enrichment at 3 Ma would therefore require a negative shift to raw $\delta^{18}O$ values. Uncertainty in the corrected $\delta^{18}O$ value is based on error propagation of Eq. (1), assuming ±1 SE for $\delta^{18}O_{bone}$ and $\delta^{13}C_{bone}$, and a ±0.1 (1s) uncertainty in the value of the correction factor. The uncertainty in $\delta^{13}C_{marine}$ is assumed to be negligible.

Although small, an additional correction should be applied for the temperature of diagenetic alteration and fossilization. Here, it is assumed that the CO_3 component of phosphates follows a temperature-dependence similar to that of carbonates. Between 0 and 25 °C, the dependencies of $\delta^{18}O$ and $\delta^{13}C$ on T for calcite are −0.22‰/°C (Kim and O'Neil, 1997) and −0.12‰/°C (Romanek et al., 1992), respectively. The total effect is small because each correction offsets the other. Temperature changes (corresponding to isotopic shifts) are referenced to MAT = 17 °C for 19–24 Ma (Retallack et al., 1999), yielding the complete correction equation

$$\delta^{18}O_{Corrected}(‰) = \delta^{18}O_{bone} + 0.22 \cdot (T - 17) - 1.25 \cdot [\delta^{13}C_{bone} + 0.12 \cdot (T - 17) + 11.0 - \delta^{13}C_{marine}] \quad (2a)$$

or, more simply

$$\delta^{18}O_{Corrected}(‰) = \delta^{18}O_{bone} + 0.07 \cdot (T - 17) - 1.25 \cdot [\delta^{13}C_{bone} + 11.0 - \delta^{13}C_{marine}] \quad (2b)$$

Estimates for MATs are: 26–29 Ma = 15 °C, 15–16 Ma = 18 °C; 10–11 Ma = 15 °C, 7–8 Ma = 15 °C, 3.2 Ma = 13 °C, <3.2 Ma = 10 °C (Kohn et al., 2002). An uncertainty in estimated temperature of ±1 °C (±1σ) contributes a ±0.07‰ uncertainty in corrected $\delta^{18}O_{bone}$, which is strongly subsidiary to the ±0.3–0.8‰ uncertainty arising from compositional variations among samples and the correction factor (Table 1).

Corrected values for $\delta^{18}O$ (Fig. 5) have two major implications. First, the isotopic shift to meteoric water across the late Oligocene warming event at 25–26 Ma was $\leqslant 1.5 \pm 0.4‰$ (±1 SE), not 2‰ as suggested by the raw data. If this shift were entirely due to temperature, then typical temperature coefficients for meteoric water of ~0.35‰/°C (Kohn et al., 2002) imply a temperature shift of ~4 ± 1 °C. Accounting for a simultaneous ~1‰ decrease in ocean $\delta^{18}O$ (Zachos et al., 2001) would increase this estimate to ~7 °C. These estimates are speculative because they are dependent on (unknown) variations in moisture sources and degrees of rainout. However, the isotopic corrections are only weakly dependent on assumed temperature. Thus, taking into account a larger temperature difference in the corrections in Eq. (2) increases the apparent isotopic shift to meteoric water to ~1.7‰, which increases the apparent temperature shift by only 1 °C.

More importantly, the corrected compositions indicate a 4–5‰ depletion in meteoric water after 7 Ma that closely parallels tooth enamel isotopic trends. In this case, regional cooling can produce a shift to meteoric water of only ~−1‰ (Kohn et al., 2002), so these data instead reflect the isotopic effect of increasing rainout over the progressively rising Cascade Range. Using a modern isotopic lapse rate across the range [7‰/1600 m; Kohn et al., 2002], a residual 3–4‰ depletion implied in meteoric water $\delta^{18}O$ indicates a 700–900 m increase in elevation since 7 Ma, i.e., approximately doubling the height of the range since the late Miocene. This trend corresponds well with initiation of Eastern Cascade volcanism, a shift to an extensional regime possibly associated with impingement of Basin and Range extension on the arc, and progressive development of the modern high range (Kohn et al., 2002). Geomorphological studies also indicate surface uplift by 700–800 m since ~5 Ma (Conrey et al., 2002), consistent with the interpretations of stable isotopes.

6. Conclusions

The basic hypothesis is verified that stable isotope compositions of the CO_3 component of fossil bone apatite are correlated with climate. $\delta^{13}C$ values correlate strongly with aridity, whereas $\delta^{18}O$ values reflect combination of source water composition (presumably meteoric water) plus evaporative enrichment. Thus, fossil bone shows promise as a terrestrial paleoclimate indicator, but will require consideration of both isotopic systems to distinguish aridity effects from changes in biomass (e.g., C3 vs. C4) and meteoric water compositions. Given an apparent timescale for fossilization of 20–50 kyr, paleoclimate changes on timescales >100 kyr can be studied. Although fossil bone may not be a ubiquitous terrestrial proxy, it has two main advantages. First, possible links between biotic evolution and climate change require proxies in fossiliferous strata. However, pedogenic minerals are not always present, and tooth enamel cannot always be sacrificed for isotopic analysis because of its taxonomic significance. In these instances, bone scrap may provide a useful and readily expendable resource for isotope analysis. Second, bone has the practical advantage that paleontologists are already well attuned to it, and can readily collect it in the field in collaboration with isotope geochemists. It is hoped that improved synergy between paleontologists and geochemists fostered

by this study will ultimately yield new insights into links among changes in paleoclimate, paleoecology, and faunas.

Acknowledgments

This material is based upon work supported by the National Science Foundation under Grant number EAR 0304181. Scott Foss is especially thanked for his gracious help with the John Day Fossil Beds Museum collections, and for longstanding field assistance. Jim Martin is thanked for providing fossil teeth from Fossil Lake, Oregon, and John Zancanella, Ted Fremd, and Diane Pritchard are thanked for permitting sample collection on federal lands. Reviews by A. Zazzo, D. Fox, J. Horita, and several anonymous reviewers greatly improved the content and discussion, but not all reviewers agree with the conclusions of this work.

Associate editor: Juske Horita

Appendix A. Methods and samples

Two to five milligram pieces of fossil bone were sawn from each larger bone fragment, and identified as either compact (cortical) or spongy (cancellous) based on location within the bone and on porosity. Each sample was then ground in a ceramic mortar and processed for isotopic analysis as described by Koch et al. (1997), using the Ca-acetate buffer and H_2O_2 pretreatments. $\delta^{18}O$ (V-SMOW) and $\delta^{13}C$ (V-PDB) compositions of phosphate standard NBS-120c ($n = 14$) were $28.25 \pm 0.12‰$ and $-6.56 \pm 0.04‰$ ($\pm 1\sigma$), respectively.

A.1. John Day Formation

Most samples were obtained in situ from paleosols collected by Retallack (2004), and allowed compositional comparison of bone carbonate with paleosol compositions from parallel transects reported by Retallack et al. (2004). These correspond with layers G through M of the Turtle Cove and Kimberly Members, plus the overlying Haystack Valley Member. In addition, samples were surface collected from layers A through F of the Turtle Cove member not sampled by Retallack et al. (2004). The age model is based on Retallack et al. (2004), which includes several high-precision $^{40}Ar/^{39}Ar$ ages on intercalated tuffs and magnetostratigraphy. Note that there are some slight discrepancies among the age model of Retallack (2004), the ages published in Retallack et al. (2004), and age linearity. Regression of Retallack et al's published ages yields the following age equation, which was used for estimating ages of fossils:

$$\text{Age (Ma)} = 28.756 - 0.01858x,$$

where x is the height above the Picture Gorge Tuff (a prominent marker horizon). This model reproduces well the expected ages of stratigraphically higher units based on biostratigraphy.

A.2. Mascall Formation

Samples were surface collected from levels 130 m through 260 m of Bestland et al. (2005; see also Fremd et al., 1997). These are equivalent to the Mascall Tuff (dated at 15.77 ± 0.04 Ma; Swisher, 1992), the overlying Red Hills sections, which are believed to correspond with the mid-Miocene climatic optimum, and ~50 m of overlying section. The uppermost samples have an estimated age of 15.2 Ma (Tedford et al., 2004).

A.3. Juntura Formation

Samples were surface collected every 3–4.5 m over a thickness of ~75 m, through the lower ~2/3 of the upper member. In contrast to other sections, which are predominantly terrestrial, the Juntura Formation consists of intimately interlayered terrestrial sands and lacustrine diatomaceous units. The sands host the mammalian bones, whereas the lacustrine layers host the fish fossils. By sampling both mammal and fish bones, a comparison of isotopic systematics of different environments was possible.

Of all samples analyzed in this study, the age of these fossils is least well constrained, but must be older than an overlying tuff correlated with the Devine Canyon Tuff (Streck and Ferns, 2004), which has a $^{40}Ar/^{39}Ar$ single crystal date of 9.68 ± 0.03 Ma (Deino and Grunder, cited in Jordan et al., 2002 and Streck and Ferns, 2004). There are no direct chronologic constraints on the age of the base of the section, but faunal lists (Shotwell, 1963) indicate it is latest Clarendonian, or CL3 (Tedford et al., 2004), as distinguished from middle Clarendonian faunas (CL2) by first appearance datums *Hystricops* and *Platybelodon*, and from Hemphillian faunas by last appearance datums *Aelurodon* and *Ustatochoerus*. Different age constraints with differing reliability provide a maximum age for the CL3 subdivision. K–Ar dating of plagioclase from a tuff at the CL2–CL3 boundary (Evernden et al., 1964) yields an age of 10.2 Ma (age uncertainty unspecified, but at least ± 0.5 Ma, 2σ; corrected for modern decay constants according to Dalrymple, 1979). In comparison, tephrochronology of a tuff from CL2 rocks in Nevada yields an age of 10.94 ± 0.03 Ma (Perkins et al., 1998). These 2 dates then yield ages for the samples (i.e., for the lower 2/3 of the upper Juntura) that are as old as 10.9–10.1 Ma (11.2 kyr/m), or as young as 10.2–9.85 Ma (4.6 kyr/m). In this study, the older age is used because the constraint is more clearly defined, and because effects of excess ^{40}Ar and/or inheritance are not known for K–Ar ages. However, this preference likely overestimates the age and duration of sedimentation. Each 3–4.5 m level then represents $\leqslant$30–50 kyr.

A.4. Rattlesnake Formation

Samples were surface collected from near the base of the Rattlesnake to just below the Rattlesnake ashflow tuff (RAFT), dated at 7.2 Ma. The age of the base of the Rattlesnake is estimated at ~7.8 Ma (Tedford et al., 2004).

A.5. Hagerman samples (Glenns Ferry Formation)

Compositions correspond to a bone sample provided by P. Gensler from the Hagerman horse quarry, with an interpolated date (between tuffs) of 3.2 ± 0.1 Ma (Hart and Brueseke, 1999).

A.6. Fossil lake samples

Dentine was sampled from fossil teeth provided by J. Martin from different layers dated via tephrochronology for the top, middle, lower, and base at ~25, ~50, ~100, and ~650 ka, respectively (Martin et al., 2005). The specific layers for the fossil bone fragments are not known.

Fossil bone $\delta^{13}C$ and $\delta^{18}O$ compositions

Compact or Spongy/Compact				Spongy or Spongy/Compact			
Sample	$\delta^{13}C$	$\delta^{18}O$	Age (Ma)	Sample	$\delta^{13}C$	$\delta^{18}O$	Age (Ma)
John Day Formation between 30.0 and 28.8 Ma (older than Retallack et al., 2004, samples)							
MK 7027-a1	−12.10	18.68	30.00	MK-7027-e	−10.31	17.06	29.80
MK 7027-a2	−11.75	17.89	30.00	MK-7027-f	−10.35	15.89	29.80
MK 7027-b	−10.01	19.36	29.86	MK-7027-h	−9.93	16.89	29.77
MK-7027-c	−9.31	17.39	29.86	MK-7027-l	−10.27	18.03	29.71
MK 7027-d	−11.82	17.58	29.83	MK-7028-b	−11.23	15.70	29.68
MK-7027-f	−10.81	17.61	29.80	MK-7027-k	−10.36	17.61	29.65
MK-7027-h	−11.55	19.31	29.77	MK-7027-m	−11.46	18.20	29.62
MK 7028-a	−10.49	19.32	29.74	MK-7027-q	−11.29	17.86	29.20
MK-7027-l	−10.27	18.03	29.71	MK-7027-t	−11.27	18.45	29.02
MK-7028-b	−10.77	17.64	29.68	MK 7029-n	−11.48	16.23	28.86
MK-7027 J	−9.86	17.88	29.65				
MK-7027-k	−10.36	17.61	29.65				
MK 7028-d	−10.25	19.32	29.62				
MK-7027-p	−11.81	18.27	29.62				
MK-7027-m	−11.36	17.86	29.62				
MK 7027-o	−11.88	17.74	29.62				
MK-7027-n	−11.79	14.83	29.62				
MK 7027-I	−9.99	17.28	29.59				
MK 7028-f	−10.78	18.12	29.53				
MK-7027-q	−11.02	17.90	29.20				
MK 7029-a	−11.12	17.23	29.13				
MK-7027-t	−11.48	18.20	29.05				
MK-7027-s	−11.16	17.84	29.01				
MK 7029-e	−10.94	19.18	28.99				
MK-7027-r	−11.76	17.62	28.96				
MK 7029-g	−11.71	17.33	28.96				
MK 7029-I	−9.97	17.89	28.89				
MK 7029-n	−11.24	16.99	28.86				
MK 7029-o	−10.88	14.47	28.83				
MK 7029-q	−10.99	17.32	28.80				
John Day Formation between 28.7 and 19.4 Ma (corresponds with Retallack et al., 2004)							
8194	−9.16	17.80	28.681	8193	−11.71	18.86	28.734
8195	−11.89	17.62	28.681	8240a	−9.65	18.19	28.678
8240b	−9.68	18.24	28.678	8292	−9.07	19.00	28.633
8240b	−11.57	17.93	28.678	8196	−10.52	18.12	28.590
8292	−9.40	19.06	28.633	8245	−10.21	18.18	28.575
8241	−10.04	17.84	28.592	8291	−11.57	19.20	28.572
8196	−10.85	17.81	28.590	8287	−10.10	20.08	28.553
8286	−10.56	17.45	28.553	8242a	−9.16	20.10	28.547
8287	−10.25	18.50	28.553	8186	−9.39	18.30	28.514
8242	−10.51	20.61	28.547	8187a	−9.06	18.56	28.514
8321	−11.47	19.90	28.525	8274	−8.30	19.46	28.514
8186	−9.30	18.30	28.514	8275	−9.51	17.70	28.514
8187	−8.77	18.71	28.514	8248	−9.89	19.98	28.508
8192	−10.26	19.76	28.514	8316	−10.42	18.82	28.508
8273	−10.91	18.46	28.514	8317	−9.31	17.40	28.508
8274	−8.55	19.97	28.514	8280	−11.12	20.80	28.481
8275	−10.09	17.55	28.514	8333	−10.54	17.98	28.386
8247	−10.73	18.60	28.508	8283	−10.33	18.96	28.363
8248	−10.47	19.51	28.508	8285	−10.59	18.89	28.306
8313	−11.27	17.99	28.508	8320	−10.17	20.05	28.131
8314	−8.86	18.69	28.508	8295	−10.40	18.43	27.979
8316	−10.66	18.25	28.508	8297	−10.84	18.26	27.979

(*continued on next page*)

Appendix Table (*continued*)

Compact or Spongy/Compact				Spongy or Spongy/Compact			
Sample	$\delta^{13}C$	$\delta^{18}O$	Age (Ma)	Sample	$\delta^{13}C$	$\delta^{18}O$	Age (Ma)
8252	−10.45	19.25	28.495	8299	−10.66	19.21	27.858
8251	−9.35	18.19	28.481	8301	−9.97	19.42	27.858
8280	−11.44	20.88	28.481	8304	−10.36	17.08	27.810
8254	−10.07	18.15	28.441	8306	−9.75	20.96	27.810
8257	−10.76	15.02	28.427	8307	−9.88	19.46	27.810
8197	−10.40	19.06	28.417	8327	−9.02	21.34	27.810
8333	−10.80	17.85	28.386	8308	−10.82	18.19	27.737
8283	−10.82	20.43	28.363	8309	−11.17	19.02	27.687
8258	−10.49	18.37	28.349	8102	−9.92	20.56	27.496
8319	−10.89	18.94	28.334	8159	−12.17	20.24	26.745
8285	−10.95	18.87	28.306	8105	−10.97	21.82	26.693
8320	−10.46	19.44	28.131	8124	−9.10	20.33	26.310
8201	−11.07	17.42	28.057	8125	−9.90	19.92	26.310
8202	−11.05	18.85	28.057	8126	−10.39	21.77	26.310
8295	−11.37	18.33	27.979	8127	−10.74	19.13	26.310
8297	−10.89	18.59	27.979	8142	−9.89	20.28	26.033
8300	−9.75	19.64	27.858	8143	−10.47	19.33	26.033
8303	−10.68	19.47	27.843	8335	−10.93	20.08	25.901
8304	−10.27	17.87	27.810	8337	−11.56	18.33	25.793
8305	−10.86	18.03	27.810	8150	−10.86	19.07	25.750
8326	−11.31	19.58	27.810	8268	−10.92	20.77	25.685
8327	−9.51	19.08	27.810	8154	−11.14	19.05	25.615
8325	−11.60	19.47	27.737	8156	−11.48	18.94	25.572
8309	−11.35	18.30	27.687	8157	−9.80	18.52	25.561
8102	−10.54	20.02	27.496	8216	−9.26	19.88	25.295
8159	−10.84	19.99	26.745	8222	−8.92	22.46	25.243
8105	−11.22	21.23	26.693	8165	−10.39	18.70	25.189
8108	−11.10	19.38	26.340	8229	−9.99	19.56	25.020
8125	−9.62	20.20	26.310	8172	−10.52	18.81	24.914
8127	−10.82	18.73	26.310	8231	−10.86	20.44	24.072
8137b	−11.93	19.32	26.295	8234	−10.80	20.29	23.912
8137	−10.26	19.38	26.295	8103	−9.39	21.17	23.654
8238	−11.21	19.27	26.182	9198	−9.12	21.52	23.080
8141	−11.14	19.62	26.033	9200	−9.86	21.88	23.080
8142	−10.22	19.86	26.033	9096	−8.24	22.19	22.314
8143	−10.66	18.97	26.033	9208	−11.30	20.43	20.058
8336	−10.39	18.71	25.866	9209	−9.24	21.10	20.058
8145	−10.60	20.15	25.840	9211	−9.00	21.01	19.802
8337	−11.05	20.06	25.793	9212	−9.86	21.34	19.802
8151	−11.45	19.07	25.775	9213	−8.97	20.85	19.802
8149	−10.41	19.84	25.750	9217	−9.96	20.34	19.775
8268	−10.56	20.05	25.685	9203	−10.04	20.15	19.382
8156	−10.29	19.42	25.572	9205	−9.36	20.54	19.382
8157	−10.03	18.27	25.561				
8207	−10.74	18.30	25.351				
8208	−10.87	19.57	25.342				
8210	−10.78	19.81	25.321				
8261	−10.64	19.87	25.321				
8214	−10.35	19.43	25.295				
8216	−9.67	19.48	25.295				
8218	−11.29	18.77	25.280				
8163	−10.25	21.61	25.251				
8221	−10.90	18.32	25.243				
8222-b	−9.82	21.26	25.243				
8235	−10.05	20.09	25.243				
8171	−9.74	19.87	25.221				
8165	−10.11	18.83	25.189				
8170	−10.16	19.71	25.139				
8172	−10.89	18.84	24.914				
8340b	−10.63	20.08	24.611				
8339	−10.10	19.20	24.596				
8103	−9.59	20.90	23.654				
9199	−8.94	21.50	23.080				

Appendix Table (*continued*)

Compact or Spongy/Compact				Spongy or Spongy/Compact			
Sample	$\delta^{13}C$	$\delta^{18}O$	Age (Ma)	Sample	$\delta^{13}C$	$\delta^{18}O$	Age (Ma)
9196	−10.19	20.47	23.054				
9095	−8.84	22.06	22.314				
9097	−9.17	21.68	22.314				
9209	−9.57	20.64	20.058				
9212	−10.42	21.61	19.802				
9213	−9.18	20.92	19.802				
9218	−10.06	20.95	19.785				
9216	−9.15	22.03	19.775				
9202	−9.31	19.66	19.528				
9204	−9.03	21.65	19.382				
Mascall Formation between 15.2 and 15.8 Ma							
70222A-1	−8.96	20.58	15.785				
70222A-2	−10.39	19.77	15.785				
70222B-1	−9.42	19.61	15.760				
70222D-2	−10.23	21.73	15.725				
70222D-3	−10.40	21.13	15.725				
70222D-4	−10.83	19.43	15.725				
70222D-1	−11.83	18.88	15.725				
70222 E-1	−10.93	22.19	15.725				
70222F-1	−10.84	21.19	15.700				
70222F-2	−9.35	21.16	15.700				
70222F-3	−10.81	20.36	15.700				
70222G-1	−10.34	20.20	15.700				
70222H-2	−11.78	20.05	15.560				
70222I-1	−10.69	20.95	15.550				
70222J-2	−11.21	20.42	15.540				
70222-k-1	−9.36	18.69	15.530				
70222-L-1	−11.01	20.94	15.520				
70222-m-1	−11.01	20.73	15.400				
70222-m-2	−10.51	20.54	15.400				
70222-n-3	−13.64	21.60	15.350				
70222-n-1	−12.86	20.51	15.350				
70222-n-2	−12.82	19.25	15.350				
70222-o	−13.12	22.14	15.340				
70222-p-1	−12.97	22.37	15.200				
Mammal (Compact)				Fish (compact)			
Juntura Formation between ~10 and ~11 Ma							
70213R	−10.03	20.93	10.10	70213Q	−4.37	19.07	10.13
70213P	−9.19	19.60	10.16	70213H	1.71	20.16	10.42
70213O	−7.49	20.91	10.20	70213F	6.58	20.04	10.49
70213N	−9.71	21.17	10.23	70213E	6.59	20.30	10.52
70213M	−10.71	20.91	10.26	70213D	7.18	20.70	10.55
70213J	−7.44	21.06	10.36	70213C	7.41	20.87	10.58
70213G	−5.55	20.94	10.46	70233G	3.93	19.50	10.60
70213E	−7.55	21.31	10.52	70213B	9.41	20.46	10.62
70213D	−8.22	19.86	10.55	70233F	8.34	20.78	10.65
70213C	−8.38	19.30	10.58	70213A	−1.75	20.66	10.65
70213B	−8.89	19.42	10.62	70233C	9.13	19.74	10.84
70213A	−7.79	19.13	10.65	70233B	−5.08	19.63	10.89
70233F	−4.20	19.12	10.65				
Compact or Spongy/Compact				Spongy or Spongy/Compact			
Rattlesnake Formation between 7.2 and 7.8 Ma							
SF 9004	−10.03	21.39	7.20	SF 9005	−9.81	22.41	7.20
SF 9005	−9.81	20.80	7.20	MK 7024 -P	−9.84	20.90	7.23
MK 7024 -L	−9.98	20.80	7.35	MK 7024 -O	−9.66	20.28	7.26
MK 7024 -K	−10.29	19.32	7.38	MK 7024 -N	−10.51	18.54	7.29
MK 7024 -I	−11.03	19.64	7.38	MK 7024 -M	−10.35	20.38	7.32
MK 7024 -H	−11.09	17.67	7.41	MK 7024 -J	−10.59	18.94	7.38
MK 7024 -G	−10.60	19.78	7.41	MK 7024 -H	−10.99	18.13	7.41
MK 7024 -E	−9.59	18.96	7.47	MK 7024 -G	−9.75	19.71	7.41
MK 7024 -D	−9.65	22.50	7.47	MK 7024 -F	−9.24	20.55	7.44

(*continued on next page*)

Appendix Table (*continued*)

Compact or Spongy/Compact				Spongy or Spongy/Compact			
Sample	$\delta^{13}C$	$\delta^{18}O$	Age (Ma)	Sample	$\delta^{13}C$	$\delta^{18}O$	Age (Ma)
MK 7024 -C	−10.06	19.76	7.47	MK 7024 -E	−9.91	18.67	7.47
MK 7024 -S	−11.53	18.89	7.62	MK 7024 -A	−9.61	21.54	7.53
MK 7024 -Y	−10.71	22.05	7.74	MK 7024 -Q	−9.72	21.31	7.59
MK 7025	−11.35	19.69	7.77	MK 7024 -R	−11.59	17.83	7.62
SF 9003	−11.85	18.08	7.80	MK 7024 -S	−11.26	17.91	7.62
				MK 7024 -T	−9.64	19.62	7.65
				MK 7024 -U	−10.69	19.63	7.65
				MK 7024 -V	−11.37	19.80	7.68
				MK 7024 -W	−11.23	20.03	7.68
				MK 7024 -X	−10.98	17.88	7.71
				SF 9002	−10.52	18.96	7.80
Hagerman, Idaho, fossils, ~3.2 Ma							
H-1	−7.76	17.72		H-1	−7.24	19.10	
H-1	−8.90	19.12		H-1	−8.13	18.72	
H-1	−9.15	20.10		H-1	−8.29	19.14	
H-1	−8.67	21.15		H-1	−6.37	21.33	
H-1	−7.13	21.86		H-1	−6.16	22.03	
H-1	−7.96	19.46		H-1	−7.78	20.33	
				H-1	−6.44	20.45	
Dentine				Compact			
Fossil Lake, Oregon, fossils, <23 to 650 ka							
FL-S-G	−4.92	22.63		FL-1	−2.74	27.04	
FL-S-G	−3.56	21.77		FL-1	−2.83	26.80	
FL-S-G	−4.35	21.13		FL-1	−2.79	27.50	
FL-S-G	−3.31	20.89		FL-1	−2.75	27.39	
FL-S-L	−7.06	20.03		FL-1	−2.48	26.98	
FL-S-L	−5.90	20.24		FL-1	−2.41	27.44	
FL-S-L	−6.54	20.20		FL-1	−2.35	27.13	
FL-S-L	−5.47	20.71		FL-1	−2.47	26.63	
FL-S-F	−4.48	19.45		FL-1	−2.59	26.96	
FL-S-F	−3.55	20.55		8059f	−2.05	27.06	
FL-S-F	−3.89	20.74		80512c	−2.85	25.35	
FL-S-F	−3.88	20.85		8058a	−3.54	28.14	
FL-S-F	−3.79	21.13		8057a	−2.09	26.03	
FL-S-WAL	−8.50	20.33		80512e	−2.99	27.05	
FL-S-WAL	−8.77	20.76		8056a	−3.84	27.33	
FL-S-WAL	−8.26	21.69		80510h	−3.72	25.92	
FL-S-WAL	−7.57	21.77		80510j	−1.00	26.04	
FL-S-WAL	−8.26	21.69		8056b	−2.67	27.16	
FL-S-WAL	−8.26	21.69		8057b	−1.58	27.52	
FL-S-G	−4.92	22.63		8059e	−3.22	27.28	
FL-S-G	−3.56	21.77		8059i	−3.70	28.51	

Note. Sample numbers are from Retallack et al. (2004) and Retallack (2004).

References

Amundson, R.G., Chadwick, O.A., Sowers, J.M., Doner, H.E., 1988. Relationship between climate and vegetation and the stable carbon isotope chemistry of soils in the eastern Mojave Desert, Nevada. *Quaternary Research* **29**, 245–254.

Amundson, R.G., Chadwick, O.A., Sowers, J.M., Doner, H.E., 1989. The stable isotope chemistry of pedogenic carbonates at Kyle Canyon, Nevada. *Soil Science Society of America Journal* **53**, 201–210.

Ayliffe, L.K., Chivas, A.R., Leakey, M.G., 1994. The retention of primary oxygen isotope compositions of fossil elephant skeletal phosphate. *Geochimica et Cosmochimica Acta* **58**, 5291–5298.

Barrick, R.E., Showers, W.J., 1994. Thermophysiology of Tyrannosaurus rex: evidence from oxygen isotopes. *Science* **265**, 222–224.

Bestland, E.A., Forbes, M.S., Krull, E.S., Retallack, G.J., Fremd, T.J., in press. Stratigraphy, Sedimentology, and Geochemistry of the Mid-Miocene Mascall Formation (Type Area, Central Oregon, USA). *PaleoBios*.

Blake, R.E., O'Neil, J.R., Garcia, G.A., 1997. Oxygen isotope systematics of microbially mediated reactions of phosphate I.: degradation of organophosphorus compounds. *Geochimica et Cosmochimica Acta* **61**, 4411–4422.

Blake, R.E., O'Neil, J.R., Garcia, G.A., 1998. Effects of microbial activity on the $\delta^{18}O$ of dissolved inorganic phosphate and textural features of synthetic apatites. *American Mineralogist* **83**, 1516–1531.

Bryant, J.D., Koch, P.L., Froelich, P.N., Showers, W.J., Genna, B.J., 1996. Oxygen isotope partitioning between phosphate and carbonate in mammalian apatite. *Geochimica et Cosmochimica Acta* **60**, 5145–5148.

Cerling, T.E., Quade, J., 1993. Stable carbon and oxygen isotopes in soil carbonates. In: Swart, P.K., Lohmann, K.C., McKenzie, J.A., Savin, S. (Eds.), *Climate Change in Continental Isotopic Records*, vol. 78. American Geophysical Union, pp. 217–231.

Clyde, W.C., Sheldon, N.D., Koch, P.L., Gunnell, G.F., Bartels, W.S., 2001. Linking the Wasatchian/Bridgerian boundary to the Cenozoic global climate optimum; new magnetostratigraphic and isotopic results from South Pass, Wyoming. *Palaeogeography, Palaeoclimatology, Palaeoecology* **167**, 175–199.

Conrey, R.M., Taylor, E.M., Donnelly-Nolan, J.M., Sherrod, D.R., 2002. North-central Oregon Cascades: exploring petrologic and tectonic intimacy in a propagating intra-arc rift. In: Moore, G.W. (Ed.), *Field Guide to Geologic Processes in Cascadia*. Oregon Department of Geology and Mineral Industries, pp. 47–90.

Dalrymple, G.B., 1979. Critical tables for conversion of K–Ar ages from old to new constants. *Geology* **7**, 558–560.

Driessens, F.C.M., Verbeeck, R.M.H., 1990. *Biominerals*. CRC Press, Boca Raton, FL.

Eppell, S.J., Tong, W., Katz, J.L., Kuhn, L., Glimcher, M.L., 2001. Shape and size of isolated bone mineralites measured using atomic force microscopy. *Journal of Orthopaedic Research* **19**, 1027–1034.

Evernden, J.F., Savage, D.E., Curtis, G.H., James, G.T., 1964. Potassium–argon dates and the Cenozoic mammalian chronology of North America. *American Journal of Science* **262**, 145–198.

Farquhar, G.D., Ehleringer, J.R., Hubick, K.T., 1989. Carbon isotope discrimination and photosynthesis. *Annual Reviews of Plant Physiology and Plant Molecular Biology* **40**, 503–537.

Fields, P.F., 1996. The Succor Creek flora of the Middle Eocene Sucker Creek Formation, Southwestern Idaho and Eastern Oregon: systematics and paleoecology. Ph.D., Michigan State University.

Fremd, T., Bestland, E.A., Retallack, G.J., 1997. John Day Basin Paleontology. *Northwest Interpretive Association*.

Hart, W.K., Brueseke, M.E., 1999. Analysis and dating of volcanic horizons from Hagerman Fossil Beds National Monument and a revised interpretation of eastern Glenns Ferry Formation chronostratigraphy. National Park Service internal report.

Iacumin, P., Bocherens, H., Mariotti, A., Longinelli, A., 1996. Oxygen isotope analyses of co-existing carbonate and phosphate in biogenic apatite; a way to monitor diagenetic alteration of bone phosphate? *Earth and Planetary Science Letters* **142**, 1–6.

Jordan, B.T., Streck, M.J., Grunder, A.L., Moore, G.W., 2002. Bimodal volcanism and tectonism of the High Lava Plains, Oregon. *Special Paper—Oregon, Department of Geology and Mineral Industries* **36**, 23–46.

Keeley, J.E., Rundel, P.W., 2003. Evolution of CAM and C4 carbon-concentrating mechanisms. *International Journal of Plant Science* **164**, S55–S77.

Kim, S.-T., O'Neil, J.R., 1997. Equilibrium and nonequilibrium oxygen isotope effects in synthetic carbonates. *Geochimica et Cosmochimica Acta* **61**, 3461–3475.

Koch, P.L., 1998. Isotopic reconstruction of past continental environments. *Annual Review of Earth and Planetary Sciences* **26**, 573–613.

Koch, P.L., Tuross, N., Fogel, M.L., 1997. The effects of sample treatment and diagenesis on the isotopic integrity of carbonate in biogenic hydroxylapatite. *Journal of Archaeological Science* **24**, 417–429.

Kohn, M.J., 1996. Predicting animal $d^{18}O$: Accounting for diet and physiological adaptation. *Geochimica et Cosmochimica Acta* **60**, 4811–4829.

Kohn, M.J., Cerling, T.E., 2002. Stable isotope compositions of biological apatite. *Reviews in Mineralogy and Geochemistry* **48**, 455–488.

Kohn, M.J., Fremd, T.J., 2006. Tectonic controls on isotope compositions and species diversification, John Day Basin, central Oregon. *PaleoBios*, in press.

Kohn, M.J., Schoeninger, M.J., Barker, W.W., 1999. Altered states: effects of diagenesis on fossil tooth chemistry. *Geochimica et Cosmochimica Acta* **18**, 2737–2747.

Kohn, M.J., Miselis, J.L., Fremd, T.J., 2002. Oxygen isotope evidence for progressive uplift of the Cascade Range, Oregon. *Earth and Planetary Science Letters* **204**, 151–165.

Land, L.S., Lundelius Jr., E.L., Valastro, S., 1980. Isotopic ecology of deer bones. *Palaeogeography, Palaeoclimatology, Palaeoecology* **32** (1–2), 143–151.

Lee-Thorpe, J.A., van der Merwe, N.J., 1991. Aspects of the chemistry of modern and fossil biogenic apatites. *Journal of Archaeological Science* **18**, 343–354.

Martin, J.E., Patrick, D., Kihm, A.J., Foit, F.F., Grandstaff, D.E., 2005. Lithostratigraphy, tephrostratigraphy, and Rare Earth Element geochemistry of fossils at the classical Pleistocene Fossil Lake area, south central Oregon. *Journal of Geology* **113**, 139–155.

Metzger, C.A., Terry, D.O.J., Grandstaff, D.E., 2004. Effect of paleosol formation on rare earth element signatures in fossil bone. *Geology* **32**, 497–500.

Millard, A.R., Hedges, R.E.M., 1999. A diffusion–adsorption model of uranium uptake by archaeological bone. *Geochimica et Cosmochimica Acta* **60**, 2139–2152.

Nelson, B.K., DeNiro, M.J., Schoeninger, M.J., 1986. Effects of diagenesis on strontium, carbon, nitrogen, and oxygen concentration and isotopic composition of bone. *Geochimica et Cosmochimica Acta* **50**, 1941–1949.

O'Leary, M.H., 1988. Carbon isotopes in photosynthesis. *Bioscience* **38**, 328–336.

Pasteris, J.D., Wopenka, B., Freeman, J.J., Rogers, K., Valsami-Jones, E., van der Houwen, J.A.M., Silva, M.J., 2004. Lack of OH in nanocrystalline apatite as a function of degree of atomic order: implications for bone and biomaterials. *Biomaterials* **25**, 229–238.

Perkins, M.E., Brown, F.H., Nash, W.P., McIntosh, W., Williams, S.K., 1998. Sequence, age, and source of silicic fallout tuffs in middle to late Miocene basins of the northern Basin and Range Province. *Geological Society of America Bulletin* **110**, 344–360.

Quade, J., Cerling, T.E., Bowman, J.R., 1989. Systematic variations in the carbon and oxygen isotopic composition of pedogenic carbonate along elevation transects in the southern Great Basin, United States. *Geological Society of America Bulletin* **101**, 464–475.

Retallack, G.J., 2001. Soils of the Past. *Blackwell Science*.

Retallack, G.J., 2004. Late Oligocene bunch grassland and early Miocene sod grassland Paleosols from central Oregon, USA. *Palaeogeography, Palaeoclimatology, Palaeoecology* **207**, 203–237.

Retallack, G.J., Bestland, E.A., Fremd, T.J., 1999. Eocene and Oligocene Paleosols of central Oregon. *Special Paper—Geological Society of America* **344**, 192.

Retallack, G.J., Tanaka, S., Tate, T., 2002. Late Miocene advent of tall grassland paleosols in Oregon. *Palaeogeography, Palaeoclimatology, Palaeoecology* **183**, 329–354.

Retallack, G.J., Wynn, J.G., Fremd, T.J., 2004. Glacial-interglacial-scale paleoclimatic change without large ice sheets in the Oligocene of central Oregon. *Geology* **32**, 297–300.

Romanek, C.S., Grossman, E.L., Morse, J.W., 1992. Carbon isotopic fractionation in synthetic aragonite and calcite; effects of temperature and precipitation rate. *Geochimica et Cosmochimica Acta* **56**, 419–430.

Rubin, M.A., Jasiuk, I., Taylor, J., Rubin, J., Ganey, T., Apkarian, R.P., 2003. TEM analysis of the nanostructure of normal and osteoporotic human trabecular bone. *Bone* **33**, 270–282.

Rubin, M.A., Rubin, J., Jasiuk, I., 2004. SEM and TEM study of the hierarchical structure of C57BL/6J and C3H/H3J mice trabecular bone. *Bone* **35**, 11–20.

Schoeninger, M.J., Deniro, M.J., 1982. Carbon isotope ratios of apatite from fossil bone cannot be used to reconstruct diets of animals. *Nature* **297** (5867), 577–578.

Shanley J.B. et al., 1998. Isotopes as indicators of environmental change. In: Kendall, C., McDonnell, J.J. (Eds.), *Isotope Tracers in Catchment Hydrology*, Elsevier, pp. 761–816.

Shotwell, J.A., 1963. The Juntura Basin; studies in earth history and paleoecology. *Transactions of the American Philosophical Society* **53**, 1–77.

Staron, R., Grandstaff, B., Gallagher, W., Grandstaff, D.E., 2001. REE signals in vertebrate fossils from Sewel, NJ: Implications for location of the K-T boundary. *Palaios* **16**, 255–265.

Staudigel, H., Doyle, P., Zindler, A., 1985. Sr and Nd isotope systematics in fish teeth. *Earth and Planetary Science Letters* **76**, 45–56.

Streck, M., Ferns, M., 2004. The Rattlesnake tuff and other Miocene silicic volcanism in eastern Oregon. In: Haller K.M., Wood, S.H.

(Eds.), *Geological Field Trips in southern Idaho, eastern Oregon, and northern Nevada; USGS Open-file Report 2004–1222*, pp. 4–19.

Swart, P.K., Lohmann, K.C., McKenzie, J.A., Savin, S., 1993. *Climate change in continental isotopic records*. American Geophysical Union.

Swisher, C.C.I., 1992. $^{40}Ar/^{39}Ar$ dating and its application to the calibration of the North American land-mammal ages. Ph.D., University of California—Berkeley.

Tedford, R.H., Albright III, L.B., Barnosky, A.D., Ferrusquia-Villafranca, I., Hunt Jr., R.M., Storer, J.E., Swisher III, C.C., Voorhies, M.R., Webb, S.D., Whistler, D.P., 2004. Mammalian biochronology of the Arikareean through Hemphillian interval (late Oligocene through early Pliocene epochs). In: Woodburne, M.O. (Ed.), *Late Cretaceous and Cenozoic mammals of North America; biostratigraphy and geochronology*. Columbia University Press, pp. 169–231.

Trueman, C.N., Benton, M.J., 1997. A geochemical method to trace the taphonomic history of reworked bones in sedimentary settings. *Geology* **25**, 263–266.

Trueman, C.N., Tuross, N., 2002. Trace elements in recent and fossil bone apatite. *Reviews in Mineralogy and Geochemistry* **48**, 489–521.

Trueman, C.N.G., Chenery, C., Eberth, D.A., Spiro, B., 2003. Diagenetic effects on the oxygen isotopic composition of bones of dinosaurs and other vertebrates recovered from terrestrial and marine sediments. *Journal of the Geological Society, London* **160**, 895–901.

Trueman, C.N.G., Behrensmeyer, A.K., Tuross, N., Weiner, S., 2004. Mineralogical and compositional changes in bones exposed on soil surfaces in Amboseli National Park, Kenya: diagenetic mechanisms and the role of sediment pore fluids. *Journal of Archaeological Sciences* **31**, 721–739.

Tuross, N., Behrensmeyer, A.K., Eanes, E.D., 1989. Strontium increases and crystallinity changes in taphonomic and archaeological bone. *Journal of Archaeological Science* **16**, 661–672.

Wang, Y., Cerling, T.E., 1994. A model for fossil tooth and bone diagenesis: implications for paleodiet reconstruction from stable isotopes. *Palaeogeography, Palaeoclimatology, Palaeoecology* **107**, 281–289.

Wilson, E.E., Awonusi, A., Morris, M.D., Kohn, D.H., Tecklenburg, M.M., Beck, L.W., 2005. Highly ordered interstitial water observed in bone by nuclear magnetic resonance. *Journal of Bone and Mineral Research* **20**, 625–634.

Wright, L.E., Schwarcz, H.P., 1996. Infrared and isotopic evidence for diagenesis of bone apatite at Dos Pilas, Guatemala: palaeodietary implications. *Journal of Archaeological Sciences* **23**, 933–944.

Wright, J., Seymour, R.S., Shaw, H.F., 1984. REE and Nd isotopes in conodont apatite; variations with geological age and depositional environment. In: Clark, D.L. (Ed.), *Conodont Biofacies and Provincialism*, vol. 196. Geological Society of America, pp. 325–340.

Zachos, J., Pagani, M., Sloan, L., Thomas, E., Billups, K., 2001. Trends, rhythms, and aberrations in global climate 65 Ma to present. *Science* **292**, 686–693.

Zazzo, A., Lécuyer, C., Mariotti, A., 2004a. Experimentally controlled carbon and oxygen isotope exchange between bioapatites and water under inorganic and microbially mediated conditions. *Geochimica et Cosmochimica Acta* **68**, 1–12.

Zazzo, A., Lécuyer, C., Sheppard, S.M.F., Grandjean, P., Mariotti, A., 2004b. Diagenesis and reconstruction of paleoenvironments: a method to restore original $\delta^{18}O$ values of carbonate and phosphate from fossil tooth enamel. *Geochimica et Cosmochimica Acta* **68**, 2245–2258.